
Article:
Li, M., Zhang, B. orcid.org/0000-0002-6472-5313, Zhang, B. et al. (5 more authors) (2023) Multi-carrier based positional modulation design with discrete phase values for metasurface elements. Digital Signal Processing. 104047. ISSN 1051-2004

https://doi.org/10.1016/j.dsp.2023.104047

Multi-carrier Based Positional Modulation Design with Discrete Phase Values for Metasurface Elements

Maolin Li[a], Bo Zhang[a,*], Baoju Zhang[a,*], Wei Liu[b], Taekon Kim[c], Wei Wang[d], Xiaonan Zhao[a], Cheng Wang[a]

[a] *Tianjin Key Laboratory of Wireless Mobile Communications and Power Transmission, College of Electronic and Communication Engineering, Tianjin Normal University, Tianjin 300387, China*

[b] *Communications Research Group, Department of Electronic and Electrical Engineering, University of Sheffield, Sheffield S1 4ET, United Kingdom*

[c] *Department of Electronics and Information Engineering, Korea University, Korea*

[d] *Sitonholy (Tianjin) Technology Co., Ltd.*

Abstract

Positional modulation (PM) as an extension of directional modulation (DM) can transmit information to the desired position(s) with known constellation mappings, but with scrambled ones in other areas. In this paper, a multi-carrier based PM design is proposed with practical discrete phase values for the employed reconfigurable metasurface, where multiple signals can be transmitted to the desired position(s) at multiple frequencies over a single channel simultaneously, and the traditional narrowband single-carrier transmission can be considered as a special case. Design examples for both the single-carrier and multi-carrier cases are provided to show the effectiveness of the proposed design.

Keywords: Positional modulation, directional modulation, multiple carriers, metasurface, discrete phase shifts.

1. Introduction

As a physical layer security technique, directional modulation (DM) can transmit the digitally modulated signal to the predetermined direction of in-

*Corresponding author: b.zhangintj@tjnu.edu.cn

Email addresses: limaolin0302@163.com (Maolin Li), wdxyzbj@163.com (Baoju Zhang), w.liu@sheffield.ac.uk (Wei Liu), taekonkim@korea.ac.kr (Taekon Kim), wangwei@aiserver.cn (Wei Wang), xiaonan5875@163.com (Xiaonan Zhao), cwang@tjnu.edu.cn (Cheng Wang)

terest and distort the constellation of the signal in other directions [1, 2, 3, 4]. In [5], a reconfigurable array of elements was designed for transmission only in a specified direction. In [6, 7], phased antenna arrays were implemented for DM where weight coefficients are optimised in the design under a required magnitude constraint. In [8], a joint optimization algorithm for designing multi-beam directional modulation (MBDM) symbols with artificial noise was introduced to ensure specific minimum error probabilities along the given eavesdropper direction. Based on phased antenna arrays, to further improve the transmission rate, an IDFT structure was employed in the DM design, where multiple-frequency signals can be transmitted to the desired direction(s) simultaneously [9]. In [10], the bit error rate (BER) performance of a system based on a two-antenna array was studied using the DM technique for eight phase shift keying modulation. In [11], A pattern synthesis approach was studied, followed by a time modulation technique for DM to form a four-dimensional (4-D) antenna array in [12]. In [13], the conditions under which legitimate users with a random frequency diverse array (DM-RFDA) system further away than eavesdroppers acquire a high level of security are investigated. In [14], two practical methods for random subcarrier selection are proposed to transmit confidential messages.

However, eavesdroppers located very close to the desired direction(s) will be a problem for the DM design, as the magnitude and phase of the received signals are similar to each other. To solve the problem, positional modulation (PM) was introduced as an extension, where signals can be transmitted to the desired position(s) with known constellation mappings, but with scrambled ones in other areas. Considering the distance dimension in PM, frequency diverse antenna arrays were introduced [15, 16, 17]. On the other hand, with the multi-path effect, phased antenna array can also be used. In [18], multiple antenna arrays at different locations were introduced to achieve PM, but the cost is high due to the implementation of multiple antenna arrays. In [19], two models based on a single carrier and multi-carrier multiple antenna arrays were proposed, and artificial noise (AN) assisted DM was used to realize secure and precise DM transmission. In [20], a hybrid single-carrier (SC) and multi-carrier (MC) system was introduced and the system security performance under various modulation modes was studied. In [21], a fixed reflecting surface with a phased antenna array was used to achieve PM, but the reflecting surface is difficult to control and not flexible enough to deal with the ever changing user conditions. Recently, reconfigurable metasurface has significant attentions in both academia and industry, since it can flexibly control the electromagnetic characteristics of the channel [22, 23, 24, 25, 26, 27, 28]. In a previous work [29], a metasuface based

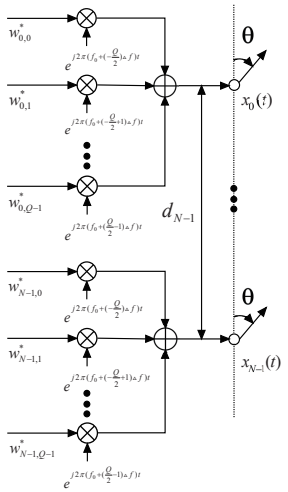

Figure 1: A multi-carrier based DM design structure.

PM design was proposed, but continuous phase shifts at the metasurface elements are assumed, which is not practical due to hardware limitations, and the design is based on a single frequency, not suitable for high data rate transmissions. To solve the problem, in this paper, a multi-carrier based PM design is introduced with discrete phase shifts constraint on metasurface elements. An iterative optimisation method with a low complexity is proposed, whose performance is compared with the exhaustive search method.

The remaining part of this paper is structured as follows. A review of multi-carrier based DM design is given in Sec. 2. A multi-carrier based PM design with discrete phase shift values for metasurface elements is presented in Sec. 3, where a single carrier design is also introduced as a special case. Design examples are provided in Sec. 4, with conclusions drawn in Sec. 5.

Notations: $(\cdot)^H$ and $(\cdot)^T$ denote the Hermitian transpose and transpose, respectively. $||\cdot||_2$ and $||\cdot||_\infty$ denote the Euclidean norm and the infinite norm respectively. $\angle\tilde{w}_{y,0}$ represents the phase of $\tilde{w}_{y,0}$ in radians. For the sake of clarity, a list of notations and variables has been provided in Table 1.

2. Review of multi-carrier based DM design

An N-element multi-carrier based antenna array (T_x) for DM is shown in Fig. 1, where each antenna is associated with multiple weight coefficients $w^*_{n,q}$, for $n = 0, \ldots, N-1$ and $q = 0, \ldots, Q-1$. Based on this structure,

Table 1: List of notations

N	Number of antennas
Y	Number of elements on the metasurface
Q	Number of subcarriers
M	Number of symbols
r	Number of desired receivers
R	Number of sampling directions
$\mathbb{F}_q$	Frequency of the q-th subcarrier
$\mathbb{E}_1, \mathbb{E}_2$	Parameters related to specific circuit and center frequency
$x_1, \bar{r}, \eta$	
$h, l, H,$	Described in Fig. 2
D_1, D_2, D_3	
$\alpha_i (i = 1, 2, \ldots, 7)$	The parameters related to specific circuit implementation
θ	Transmission angle from antenna array to the receiver
θ_{ML}	Desired directions
θ_{SL}	Un-desired directions
ζ	Angle from antenna array to metasurface
φ	Angle from metasurface to the receiver
d_n	The distance from the 0-th antenna to the n-th antenna
c	The speed of propagation
ω_q	Angular frequency of the q-th subcarrier
$w_{n,q}$	Weight coefficient for the n-th antenna at the q-th frequency
$w_{m,n,q}$	Weight coefficient for the n-th antenna corresponding to the m-th symbol at the q-th frequency
$\tilde{w}_{y,q}$	Weight coefficient for the y-th unit on metasurface at the q-th frequency
$A_{y,q}$	Amplitude reflection coefficient of the y-th metasurface element
$v_{y,q}$	Phase shift coefficient of the y-th metasurface element
$p(\omega_q, \theta)$	Beam response of the array at the q-th frequency
$p_m(\omega_q, \theta)$	Beam response of the array corresponding to the m-th symbol at the q-th frequency
$p(\omega_q, \theta, \zeta, \varphi)$	Magnitude response at desired locations
$\mathbf{s}(\omega_q, \theta)$	Steering vector from antenna array to the receiver at the q-th frequency
$\tilde{\mathbf{s}}(\omega_q, \zeta)$	Steering vector from antenna array to metasurface at the q-th frequency
$\tilde{\mathbf{s}}(\omega_q, \varphi)$	Steering vector from metasurface to the receiver at the q-th frequency
$\mathbf{w}(\omega_q)$	The set of all the $w_{n,q}$, $n = 0, 1, \ldots, N-1$
$\mathbf{w}_m(\omega_q)$	The set of all the $w_{m,n,q}$, $n = 0, 1, \ldots, N-1$
$\tilde{\mathbf{w}}(\omega_q)$	The set of all the $\tilde{w}_{y,q}$, $y = 0, 1, \ldots, Y-1$
$\mathbf{p}_m(\omega_q, \theta_{ML})$	The set of all responses in the desired directions at the q-th frequency
$\mathbf{p}_m(\omega_q, \theta_{SL})$	The set of all responses in the un-desired directions at the q-th frequency
$\mathbf{p}_m(\omega_q, \theta_{R_x}, \zeta_{R_x}, \varphi_{R_x})$	The set of all magnitude responses for the m-th symbol at the desired locations
$\mathbf{p}_m(\omega_q, \theta_{E_x}, \zeta_{E_x}, \varphi_{E_x})$	The set of all magnitude responses for the m-th symbol at the un-desired locations
$\mathbf{S}(\omega_q, \theta_{ML})$	The set of all steering vectors corresponding to the q-th frequency at the mainlobe regions
$\mathbf{S}(\omega_q, \theta_{SL})$	The set of all steering vectors corresponding to the q-th frequency at the sidelobe regions
$\mathbf{S}(\omega_q, \theta_{R_x})$	Steering matrix from antenna array to the receiver
$\mathbf{S}(\omega_q, \theta_{E_x})$	Steering matrix from antenna array to eavesdroppers
$\tilde{\mathbf{S}}(\omega_q, \zeta_{M_x})$	Steering matrix from antenna array to metasurface
$\tilde{\mathbf{S}}(\omega_q, \zeta_{R_x})$	Steering matrix from metasurface to the receiver
$\tilde{\mathbf{S}}(\omega_q, \zeta_{E_x})$	Steering matrix from metasurface to eavesdroppers

the steering vector at the q-th frequency is given by

$$\mathbf{s}(\omega_q, \theta) = [1, e^{j\omega_q d_1 \cos\theta/c}, \ldots, e^{j\omega_q d_{N-1} \cos\theta/c}]^T. \tag{1}$$

The weight vector at the q-th frequency is represented by

$$\mathbf{w}(\omega_q) = [w_{0,q}, w_{1,q}, \ldots, w_{N-1,q}]^T. \tag{2}$$

Then, the beam response of the array at the q-th frequency can be formulated as follows

$$p(\omega_q, \theta) = \mathbf{w}(\omega_q)^H \mathbf{s}(\omega_q, \theta). \tag{3}$$

In multi-carrier based DM design, for the m-th symbol at the q-th frequency ($m = 0, 1, \ldots, M-1$ for M-ary signaling and $q = 0, \ldots, Q-1$), $p_m(\omega_q, \theta)$ can be set in different groups based on the transmission angles pointing to the desired directions θ_{ML} or un-desired directions θ_{SL}. Here, considering r mainlobe directions and $R-r$ sidelobe directions, we have

$$\begin{aligned} \mathbf{p}_m(\omega_q, \theta_{ML}) =& [p_m(\omega_q, \theta_0), p_m(\omega_q, \theta_1), \ldots, \\ & p_m(\omega_q, \theta_{r-1})], \\ \mathbf{p}_m(\omega_q, \theta_{SL}) =& [p_m(\omega_q, \theta_r), p_m(\omega_q, \theta_{r+1}), \ldots, \\ & p_m(\omega_q, \theta_{R-r})] \ . \end{aligned} \tag{4}$$

Similarly, in M-ary signaling, the weight vector for the m-th symbol at the q-th frequency can be represented by $\mathbf{w}_m(\omega_q) = [w_{m,0,q}, \ldots, w_{m,N-1,q}]^T$. Moreover, $\mathbf{S}(\omega_q, \theta_{ML})$ and $\mathbf{S}(\omega_q, \theta_{SL})$ denote the steering matrices of all steering vectors at the mainlobe regions and sidelobe regions at the q-th frequency, respectively.

Then, the weight coefficient optimisation for the m-th symbol at the q-th frequency based on a given geometry is formulated by

$$\begin{aligned} \min_{\mathbf{w}_m(\omega_q)} \quad & ||\mathbf{p}_m(\omega_q, \theta_{SL}) - \mathbf{w}_m(\omega_q)^H \mathbf{S}(\omega_q, \theta_{SL})||_2 \\ \text{s. t.} \quad & \mathbf{w}_m(\omega_q)^H \mathbf{S}(\omega_q, \theta_{ML}) = \mathbf{p}_m(\omega_q, \theta_{ML}), \end{aligned} \tag{5}$$

where the cost function and the constraint in (5) ensure minimum difference between desired and designed responses in the sidelobe areas, and the same value for these two responses in the mainlobe direction.

3. Proposed multi-carrier based PM design with discrete phase shifts for metasurface

3.1. Proposed multi-carrier based PM design

The above design in (5) cannot solve the problem where eavesdroppers are very close to the desired direction(s), as their received modulation patterns are similar to each other. Therefore, in this section, we propose a multi-carrier based PM design with the aid of metasurface and the structure is shown in Fig. 2. The transmission antenna array T_x is the same as in Fig. 1, where an IDFT structure is used instead [30]. At the receiver

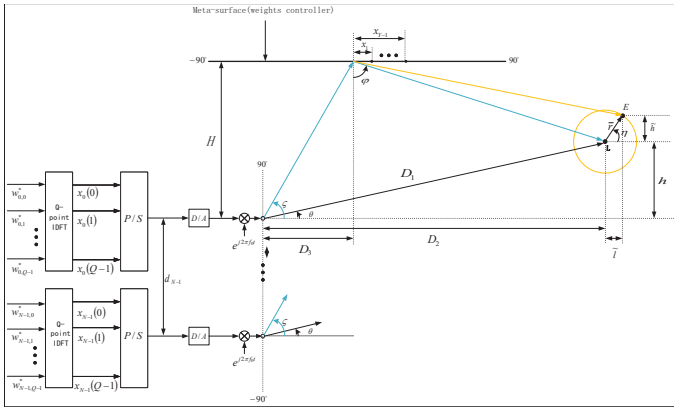

Figure 2: The proposed multi-carrier based PM structure.

side, an antenna element R_x is located at position L, while eavesdroppers E_x are located at position E close to R_x, with the radius $\bar{r}$ of the circle centre R_x and $\eta \in [0°, 360°)$. The corresponding vertical and horizontal distance are represented by $\tilde{h}$ and $\tilde{l}$, respectively. It is assumed that the specific location of the eavesdropper is uncertain at the transmitter, and E in Fig. 2 shows the situation of one sampling point. The metasurface M_x including Y electromagnetic units is implemented in the design, with a distance H away from T_x and a spacing x_y between the zeroth and the y-th unit ($y = 1, \ldots, Y-1$). The transmission angle for the direct path from T_x to R_x is represented by $\theta \in [-90°, 90°]$, while the angle for the path from T_x to M_x is represented by ζ, and the angle for the path from M_x to R_x represented by φ. The weight coefficients for the n-th antenna and the y-th electromagnetic unit on metasurface at the q-th frequency are represented by $w_{n,q}$ and $\tilde{w}_{y,q}$, respectively ($n = 0, 1, \ldots, N-1$; $y = 0, 1, \ldots, Y-1$). D_1 represents the distance from T_x to R_x, and h is the vertical distance to the broadside direction which is positive for the position above the broadside direction and negative for the position below. The projection of D_1 onto the broadside direction is represented by D_2. D_3 is the horizontal distance from the zeroth electromagnetic element to the transmitter.

With the given parameters, the steering vector for the direct path from T_x to R_x at the q-th frequency, represented by $\mathbf{s}(\omega_q, \theta)$ and the corresponding weight vector for T_x represented by $\mathbf{w}(\omega_q)$ are the same as in Eqs. (1) and (2). The steering vectors for the paths from T_x to M_x and from M_x to R_x

at the q-th frequency can be formulated as follows,

$$\begin{aligned}\hat{\mathbf{s}}(\omega_q,\zeta) &= [1, e^{j\omega_q d_1 \sin\zeta/c}, \ldots, e^{j\omega_q d_{N-1}\sin\zeta/c}]^T,\\ \tilde{\mathbf{s}}(\omega_q,\varphi) &= [1, e^{-j\omega_q x_1 \sin\varphi/c}, \ldots, e^{-j\omega_q x_{Y-1}\sin\varphi/c}]^T.\end{aligned} \tag{6}$$

The corresponding weight vector for M_x can be represented by

$$\begin{aligned}\tilde{\mathbf{w}}(\omega_q) &= [\tilde{w}_{0,q}, \tilde{w}_{1,q}, \ldots, \tilde{w}_{Y-1,q}]\\ &= [A_{0,q}e^{j\upsilon_{0,q}}, A_{1,q}e^{j\upsilon_{1,q}}, \ldots, A_{Y-1,q}e^{j\upsilon_{Y-1,q}}]\end{aligned} \tag{7}$$

where $A_{y,q} \in [0,1]$ and $\upsilon_{y,q} \in [0, 2\pi]$ are the amplitude reflection and phase shift coefficient of the y-th metasurface element ($y = 0, 1, \ldots, Y-1$). Then, the magnitude response for the desired locations can be represented by

$$\begin{aligned}p(\omega_q,\theta,\zeta,\varphi) &= \mathbf{w}(\omega_q)^H \mathbf{s}(\omega_q,\theta)\\ &\quad + (\mathbf{w}(\omega_q)^H \hat{\mathbf{s}}(\omega_q,\zeta)\cdot\tilde{\mathbf{w}}(\omega_q))\tilde{\mathbf{s}}(\omega_q,\varphi),\end{aligned} \tag{8}$$

where $\cdot$ represents the dot product. Here, we can see that there are two parts added together, where one is the response for the LOS from T_x to R_x and the other the response for reflected path via metasurface.

Similar to the previous design in DM, in PM design with M-ary signaling, we also assume r desired receivers and $R-r$ eavesdroppers with the corresponding angles θ_k, ζ_k and φ_k related to the k-th location, $k = 0, \ldots, R-1$. Then, $\mathbf{S}(\omega_q,\theta_{R_x})$, $\mathbf{S}(\omega_q,\theta_{E_x})$, $\hat{\mathbf{S}}(\omega_q,\zeta_{M_x})$, $\tilde{\mathbf{S}}(\omega_q,\varphi_{R_x})$ and $\tilde{\mathbf{S}}(\omega_q,\varphi_{E_x})$ are constructed representing the set of steering matrices for the direct path from T_x to R_x, from T_x to E_x, from T_x to M_x, from M_x to R_x, from M_x to E_x for the q-th frequency, respectively

$$\begin{aligned}\mathbf{S}(\omega_q,\theta_{R_x}) &= [\mathbf{s}(\omega_q,\theta_0), \mathbf{s}(\omega_q,\theta_1), \ldots, \mathbf{s}(\omega_q,\theta_{r-1})],\\ \mathbf{S}(\omega_q,\theta_{E_x}) &= [\mathbf{s}(\omega_q,\theta_r), \mathbf{s}(\omega_q,\theta_{r+1}), \ldots, \mathbf{s}(\omega_q,\theta_{R-1})],\\ \hat{\mathbf{S}}(\omega_q,\zeta_{M_x}) &= [\hat{\mathbf{s}}(\omega_q,\zeta_0), \hat{\mathbf{s}}(\omega_q,\zeta_1), \ldots, \hat{\mathbf{s}}(\omega_q,\zeta_{Y-1})],\\ \tilde{\mathbf{S}}(\omega_q,\varphi_{R_x}) &= [\tilde{\mathbf{s}}(\omega_q,\varphi_0), \tilde{\mathbf{s}}(\omega_q,\varphi_1), \ldots, \tilde{\mathbf{s}}(\omega_q,\varphi_{r-1})],\\ \tilde{\mathbf{S}}(\omega_q,\varphi_{E_x}) &= [\tilde{\mathbf{s}}(\omega_q,\varphi_r), \tilde{\mathbf{s}}(\omega_q,\varphi_{r+1}), \ldots, \tilde{\mathbf{s}}(\omega_q,\varphi_{R-1})].\end{aligned} \tag{9}$$

Accordingly, the magnitude responses for R_x and E_x for the m-th symbol ($m = 0, 1, \ldots, M-1$) can be placed into different groups, represented by $\mathbf{p}_m(\omega_q,\theta_{R_x},\zeta_{R_x},\varphi_{R_x})$ and $\mathbf{p}_m(\omega_q,\theta_{E_x},\zeta_{E_x},\varphi_{E_x})$ based on their locations,

$$\begin{aligned}\mathbf{p}_m(\omega_q,\theta_{R_x},\zeta_{R_x},\varphi_{R_x}) &= [p_m(\omega_q,\theta_0,\zeta_0,\varphi_0), \ldots,\\ &\qquad p_m(\omega_q,\theta_{r-1},\zeta_{r-1},\varphi_{r-1})],\\ \mathbf{p}_m(\omega_q,\theta_{E_x},\zeta_{E_x},\varphi_{E_x}) &= [p_m(\omega_q,\theta_r,\zeta_r,\varphi_r), \ldots,\\ &\qquad p_m(\omega_q,\theta_{R-r},\zeta_{R-r},\varphi_{R-r})].\end{aligned} \tag{10}$$

The corresponding weight vector of T_x can be given by

$$\begin{aligned}\mathbf{w}_m(\omega_q) = [w_{m,0,q}, \ldots, w_{m,N-1,q}]^T, m = 0, 1, \ldots, M-1 \\ q = 0, 1, \ldots, Q-1.\end{aligned} \tag{11}$$

Therefore, the PM design can be formulated as

$$\begin{aligned}&\min_{\mathbf{w}_m(\omega_q), \tilde{\mathbf{w}}(\omega_q)} \sum_{m=0}^{M-1} ||\mathbf{p}_m(\omega_q, \theta_{E_x}, \zeta_{E_x}, \varphi_{E_x}) - (\mathbf{w}_m(\omega_q)^H \\ &\mathbf{S}(\omega_q, \theta_{E_x}) + (\mathbf{w}_m(\omega_q)^H \hat{\mathbf{S}}(\omega_q, \zeta_{M_x}) \cdot \tilde{\mathbf{w}}(\omega_q)) \tilde{\mathbf{S}}(\omega_q, \varphi_{E_x})||_2 \\ &\text{s.t.} \\ &\text{for} \quad m = 0, 1, \ldots, M-1 \\ &\{ \\ &\quad \mathbf{w}_m(\omega_q)^H \mathbf{S}(\omega_q, \theta_{R_x}) + (\mathbf{w}_m(\omega_q)^H \hat{\mathbf{S}}(\omega_q, \zeta_{M_x}) \cdot \tilde{\mathbf{w}}(\omega_q)) \\ &\quad \tilde{\mathbf{S}}(\omega_q, \varphi_{R_x}) = \mathbf{p}_m(\omega_q, \theta_{R_x}, \zeta_{R_x}, \varphi_{R_x}) \\ &\} \\ &||\tilde{\mathbf{w}}(\omega_q)||_\infty \leq 1,\end{aligned} \tag{12}$$

where the cost function minimises the desired and designed responses at E_x for all M symbols, and the equality constraint in the loop keeps the same desired and designed responses at R_x. The inequality constraint $||\tilde{\mathbf{w}}(\omega_q)||_\infty \leq 1$ keeps the magnitude of each metasurface element lower than 1, satisfying the amplitude reflection requirement of metasurface element in Eq. (7).

However, the phase shift of each metasurface element at the centre frequency cannot be set at any values in practice, which is controlled by tuning the bias voltage (i.e. the capacitance) of the varactor, and is usually controlled by B bits and therefore has 2^B discrete phase values [31, 32], which yields a finite set:

$$\begin{aligned}&\angle \tilde{w}_{y,0} = \upsilon_{y,0} \in [0, 2\pi/2^B, \ldots, (2^B - 1)2\pi/2^B], \\ &for \quad y = 0, \ldots, Y-1.\end{aligned} \tag{13}$$

Moreover, the above design in (12) assumes that the phase shifts and magnitude reflections for each frequency are independent, which cannot precisely describe the signal reflection by a practical IRS. Actually, the magnitude reflections and the phase shifts of metasurface at each frequency are associated with the centre frequency. The mathematical equation between the

reflection coefficients of metasurface and the carrier frequency of the incident signal has been formulated in [32], given by

$$\begin{aligned} A_{y,q} &= -\frac{\alpha_4 \upsilon_{y,0} + \alpha_7}{((\mathbb{F}_q/10^9 - \mathbb{E}_1(\upsilon_{y,0}))/0.05)^2 + 4} + 1, \\ \upsilon_{y,q} &= -2tan^{-1}[\mathbb{E}_2(\upsilon_{y,0})(\mathbb{F}_q/10^9 - \mathbb{E}_1(\upsilon_{y,0}))], \\ \mathbb{E}_1(\upsilon_{y,0}) &= \alpha_1 \tan(\upsilon_{y,0}/3) + \alpha_2 \sin(\upsilon_{y,0}) + \alpha_5, \\ \mathbb{E}_2(\upsilon_{y,0}) &= \alpha_3 \upsilon_{y,0} + \alpha_6, \\ for \quad y &= 0, \ldots, Y-1; \quad q = 1, \ldots, Q-1 \end{aligned} \tag{14}$$

where $A_{y,q}$ and $\upsilon_{y,q}$ denote the amplitude and phase value of the y-th element at the frequency $\mathbb{F}_q$. Here, $\mathbb{F}_q$ denotes the q-th frequency with $\mathbb{F}_q = f_0 + (q - \frac{Q}{2})\triangle f$ for $q = 0, 1, \ldots, Q-1$. α_i for $i = 1, 2, \ldots, 7$ are the parameters related to specific circuit implementation [32]. Therefore, the new PM design with discrete phase values for metasurface is formulated as

$$\begin{aligned} &\min_{\mathbf{w}_m(\omega_q), \tilde{\mathbf{w}}(\omega_q)} \sum_{m=0}^{M-1} ||\mathbf{p}_m(\omega_q, \theta_{E_x}, \zeta_{E_x}, \varphi_{E_x}) - (\mathbf{w}_m(\omega_q)^H \\ &\mathbf{S}(\omega_q, \theta_{E_x}) + (\mathbf{w}_m(\omega_q)^H \hat{\mathbf{S}}(\omega_q, \zeta_{M_x}) \cdot \tilde{\mathbf{w}}(\omega_q)) \tilde{\mathbf{S}}(\omega_q, \varphi_{E_x})||_2 \\ &\text{s.t.} \\ &\text{for} \quad m = 0, 1, \ldots, M-1 \\ &\{ \\ &\quad \mathbf{w}_m(\omega_q)^H \mathbf{S}(\omega_q, \theta_{R_x}) + (\mathbf{w}_m(\omega_q)^H \hat{\mathbf{S}}(\omega_q, \zeta_{M_x}) \cdot \tilde{\mathbf{w}}(\omega_q)) \\ &\quad \tilde{\mathbf{S}}(\omega_q, \varphi_{R_x}) = \mathbf{p}_m(\omega_q, \theta_{R_x}, \zeta_{R_x}, \varphi_{R_x}) \\ &\} \\ &\upsilon_{y,0} \in [0, 2\pi/2^B, \ldots, (2^B - 1)2\pi/2^B], \\ &q = 0, \ldots, Q-1. \end{aligned} \tag{15}$$

Here, we can see the differences between (15) and (12) are the cancellation of the magnitude constraint of metasurface elements, and the addition of discrete phase values for metasurface. The magnitude constraint is not needed as the magnitude in (15) is pre-calculated by (14) and its value will not exceed 1.

However, the formulation (15) is non-convex due to the discrete phase value of $\upsilon_{y,0}$ at the centre frequency f_0. To solve the problem, when B is small we can adopt the following exhaustive search method for all combinations of discrete phase shifts of metasurface elements.

1. List all 2^{BY} combinations of $\upsilon_{y,0}$ for all $y = 0, \ldots, Y-1$. Then, based on (14), we have the corresponding $\tilde{\mathbf{w}}(\omega_q)$ for all Q frequencies.
2. Based on the given set of $\tilde{\mathbf{w}}^x(\omega_0)$ at the centre frequency f_0 with the corresponding $\tilde{\mathbf{w}}(\omega_q)$ from (14) at all Q frequencies, $\mathbf{w}_m(\omega_q)$ and the corresponding cost function value C_f can be calculated by (15). Therefore, we can obtain 2^{BY} cost function values. Here, $\tilde{\mathbf{w}}^x(\omega_0)$ represents the x-th set of discrete phase shift combinations $\tilde{\mathbf{w}}(\omega_0)$, where $x = [0, 1, \ldots, 2^{BY}-1]$.
3. Select $\tilde{\mathbf{w}}^x(\omega_q)$ and $\mathbf{w}_m(\omega_q)$ for $q = 0, 1, \ldots, Q-1$ corresponding to the minimum value of cost function.

The parameter $\tilde{\mathbf{w}}^x(\omega_0)$ is used to represent the x-th set of discrete phase shift combination $\tilde{\mathbf{w}}(\omega_0)$ at the centre frequency, and $\tilde{\mathbf{w}}^x(\omega_0)$ and $\tilde{\mathbf{w}}(\omega_0)$ are the same as in (15). However, a clear problem with exhaustive search is its extremely high complexity of $O(2^{BY})$, which would be prohibitively large with a large number of metasurface elements.

To solve the problem, in this paper we propose an iterative optimisation method for weight coefficients of M_x and T_x. For two variables in the formulation (15) where the value of $\upsilon_{y,0}$ can only be selected from a few discrete values, we optimise coefficients of metasurface element one by one, and values of coefficients for T_x are calculated based on the optimised coefficients of M_x. The iterative processe is described as follows:

1. Initialize $\upsilon_{y,0} = 0$ for $y = 0, 1, \ldots, Y-1$, and then we have the corresponding $\tilde{\mathbf{w}}(\omega_q)$ for $q = 0, 1, \ldots, Q-1$.
2. Based on the given $\tilde{\mathbf{w}}(\omega_q)$, $\mathbf{w}_m(\omega_q)$ can be calculated and the corresponding cost function value is set as the minimum cost function value $C_f(\min)$.
3. Take the elements in $\upsilon_{y,0} = [0, 2\pi/2^B, \ldots, (2^B-1)2\pi/2^B]$ in turn and calculate the cost function value $C_f(\upsilon_y)$ of Eq. (15). If $C_f(\upsilon_y)$ is less than $C_f(\min)$, then take $C_f(\upsilon_y)$ as the new $C_f(\min)$ and select the corresponding $\upsilon_{y,0}$ as the new phase coefficient at the y-th element for the centre carrier frequency; otherwise, the phase coefficient at the centre carrier frequency at the y-th element does not change.
4. Repeat Step 3) for $y = 0, 1, \ldots, Y-1$. Then, the minimum cost function in this iteration can be calculated.
5. Go back to Step 3) and continue this process until the cost function converges. In this paper, we consider the cost function has converged when it does not change for three consecutive iterations.

With the above method, the minimum cost function value with the corresponding $\mathbf{w}_m(\omega_q)$ and $\tilde{\mathbf{w}}(\omega_q)$ for $q = 0, 1, \ldots, Q-1$ and $m = 0, 1, \ldots, M-1$

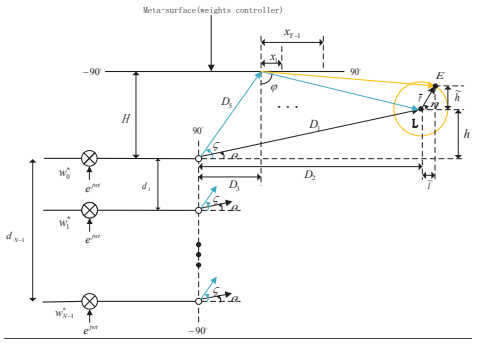

Figure 3: The single carrier based PM structure.

can be obtained. The complexity of the proposed method is $O(zBY)$ where z represents the number of iterations, and it is much lower than the exhaustive search method; the whole solution can be implemented by the CVX toolbox in MATLAB [33, 34].

Note that due to the finite discrete phase value of metasurface elements at the centre frequency, the corresponding phase value for other frequencies can be calculated, and therefore the sum of cost function values for all Q frequencies is limited and the minimum value can be selected. Our proposed method is to approximate the minimum value by iterations. In each iteration, for weight coefficient optimisation of the y-th metasurface element, the corresponding $C_f(\upsilon_y)$, which is the sum of cost function values for all Q frequencies has only two states compared to the current minimum objective function value $C_f(\min)$: state 1) larger than or equal to $C_f(\min)$; state 2) less than $C_f(\min)$. If the cost function value is in state 1), then the cost function and the corresponding phase value of metasurface element will not be updated. If the cost function value is in state 2), then we use the smaller value to replace $C_f(\min)$. By this design, the optimisation process follows a decreasing trend and is guaranteed to converge.

3.2. Single carrier based PM design as a special case

As a special case, for a single carrier PM design, the array structure is reduced to Fig. 3.

For a single frequency ω_0, Eq. (6) changes to

$$\begin{aligned} \hat{\mathbf{s}}(\omega_0, \zeta) &= [1, e^{j\omega_0 d_1 \sin\zeta/c}, \ldots, e^{j\omega_0 d_{N-1} \sin\zeta/c}]^T, \\ \tilde{\mathbf{s}}(\omega_0, \varphi) &= [1, e^{-j\omega_0 x_1 \sin\varphi/c}, \ldots, e^{-j\omega_0 x_{Y-1} \sin\varphi/c}]^T, \end{aligned} \tag{16}$$

and the weight vectors for T_x and M_x are simplified to

$$\mathbf{w}(\omega_0) = [w_{0,0}, w_{1,0}, \ldots, w_{N-1,0}]^T \tag{17}$$

$$\begin{aligned} \tilde{\mathbf{w}} &= [\tilde{w}_{0,0}, \tilde{w}_{1,0}, \ldots, \tilde{w}_{Y-1,0}] \\ &= [A_{0,0}e^{j\upsilon_{0,0}}, A_{1,0}e^{j\upsilon_{1,0}}, \ldots, A_{Y-1,0}e^{j\upsilon_{Y-1,0}}] \end{aligned} \tag{18}$$

For M-ary signaling, the weight vector for the m-th symbol for T_x can be represented by

$$\mathbf{w}_m(\omega_0) = [w_{m,0}, \ldots, w_{m,N-1}]^T, m = 0, \ldots, M-1. \tag{19}$$

With the same set of parameters as in (9) and the same assumption of r desired locations and $R-r$ eavesdroppers in the PM design, the steering matrices related to ω_0 are given by

$$\begin{aligned} \mathbf{S}(\omega_0, \theta_{R_x}) &= [\mathbf{s}(\omega_0, \theta_0), \mathbf{s}(\omega_0, \theta_1), \ldots, \mathbf{s}(\omega_0, \theta_{r-1})], \\ \mathbf{S}(\omega_0, \theta_{E_x}) &= [\mathbf{s}(\omega_0, \theta_r), \mathbf{s}(\omega_0, \theta_{r+1}), \ldots, \mathbf{s}(\omega_0, \theta_{R-1})], \\ \hat{\mathbf{S}}(\omega_0, \zeta_{M_x}) &= [\hat{\mathbf{s}}(\omega_0, \zeta_0), \hat{\mathbf{s}}(\omega_0, \zeta_1), \ldots, \hat{\mathbf{s}}(\omega_0, \zeta_{Y-1})], \\ \tilde{\mathbf{S}}(\omega_0, \varphi_{R_x}) &= [\tilde{\mathbf{s}}(\omega_0, \varphi_0), \tilde{\mathbf{s}}(\omega_0, \varphi_1), \ldots, \tilde{\mathbf{s}}(\omega_0, \varphi_{r-1})], \\ \tilde{\mathbf{S}}(\omega_0, \varphi_{E_x}) &= [\tilde{\mathbf{s}}(\omega_0, \varphi_r), \tilde{\mathbf{s}}(\omega_0, \varphi_{r+1}), \ldots, \tilde{\mathbf{s}}(\omega_0, \varphi_{R-1})]. \end{aligned} \tag{20}$$

Accordingly, the magnitude responses for the receiver side and eavesdroppers for the m-th symbol can be represented by $\mathbf{p}_m(\omega_q, \theta_{R_x}, \zeta_{R_x}, \varphi_{R_x})$ and $\mathbf{p}_m(\omega_0, \theta_{E_x}, \zeta_{E_x}, \varphi_{E_x})$, respectively.

$$\begin{aligned} \mathbf{p}_m(\omega_0, \theta_{R_x}, \zeta_{R_x}, \varphi_{R_x}) =& [p_m(\omega_0, \theta_0, \zeta_0, \varphi_0), \ldots, \\ & p_m(\omega_0, \theta_{r-1}, \zeta_{r-1}, \varphi_{r-1})], \\ \mathbf{p}_m(\omega_0, \theta_{E_x}, \zeta_{E_x}, \varphi_{E_x}) =& [p_m(\omega_0, \theta_r, \zeta_r, \varphi_r), \ldots, \\ & p_m(\omega_0, \theta_{R-r}, \zeta_{R-r}, \varphi_{R-r})]. \end{aligned} \tag{21}$$

Considering the requirements of discrete phase values for the weight coeffi-

cients of metasurface, the new formulation becomes

$$
\begin{aligned}
&\min_{\mathbf{w}_m(\omega_0),\tilde{\mathbf{w}}(\omega_0)} \sum_{m=0}^{M-1} ||\mathbf{p}_m(\omega_0,\theta_{E_x},\zeta_{E_x},\varphi_{E_x}) - (\mathbf{w}_m(\omega_0)^H \\
&\mathbf{S}(\omega_0,\theta_{E_x}) + (\mathbf{w}_m(\omega_0)^H \hat{\mathbf{S}}(\omega_0,\zeta_{M_x}) \cdot \tilde{\mathbf{w}}(\omega_0))\tilde{\mathbf{S}}(\omega_0,\varphi_{E_x})||_2 \\
&\text{s.t.} \\
&\text{for} \quad m = 0,1,\ldots,M-1 \\
&\{ \\
&\quad \mathbf{w}_m(\omega_0)^H \mathbf{S}(\omega_0,\theta_{R_x}) + (\mathbf{w}_m(\omega_0)^H \hat{\mathbf{S}}(\omega_0,\zeta_{M_x}) \cdot \tilde{\mathbf{w}}(\omega_0)) \\
&\quad \tilde{\mathbf{S}}(\omega_0,\varphi_{R_x}) = \mathbf{p}_m(\omega_0,\theta_{R_x},\zeta_{R_x},\varphi_{R_x}) \\
&\} \\
&\upsilon_{y,0} \in [0, 2\pi/2^B, \ldots, (2^B-1)2\pi/2^B],
\end{aligned}
\tag{22}
$$

The formulation (22) is still non-convex due to the discrete phase value of $\tilde{w}_{y,0}$. To solve the problem, we can adopt the aforementioned iterative optimisation method, where the design process is consistent between the single carrier and the multi-carrier based PM designs.

4. Design examples

Assume the transmitter T_x is a uniform linear array with the number of antennas $N = 19$. The metasurface M_x has $Y = 21$ electromagnetic elements with an equally spaced $x_1 = \lambda/2$ between adjacent units. One desired receiver ($r = 1$) R_x is located at the position L with $h = 20\lambda$, $H = 1000\lambda$, $D_1 = 900\lambda$ and $D_3 = 800\lambda$, and surrounded by $R = 72$ eavesdroppers at the circumference with $\bar{r} = 5\lambda$ and $\eta \in [0°, 360°)$, sampled every 5°. The desired response at R_x is a value of one in magnitude (the gain is 0dB) with 90° phase shift, i.e. symbols '00', '01', '11', '10' correspond to 45°, 135°, −135° and −45°, respectively, and a value of 0.2 (magnitude) with randomly generated phase shifts at locations of eavesdroppers.

4.1. Design example for the multi-carrier based PM design

The first design is based on the implementation $\alpha_1 = 0.2$, $\alpha_2 = -0.015$, $\alpha_3 = -0.75$, $\alpha_4 = -0.05, \alpha_5 = 2.4, \alpha_6 = 11.02$, and $\alpha_7 = 1.65$. The carrier frequency f_0 is set to 2.4GHz, with a bandwidth of 100MHz, split into 8 frequencies (8-point IDFT).

Fig. 4a shows the optimised phase value of each metasurface element at the centre frequency, i.e., the optimal phase value at the centre frequency is

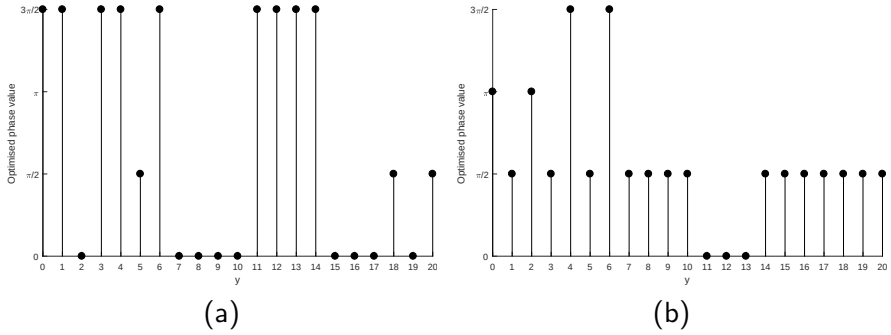

Figure 4: Optimised phase value for each metasurface element (a) at the centre frequency in the multi-carrier based PM design (15), (b) in the single carrier based PM design (22).

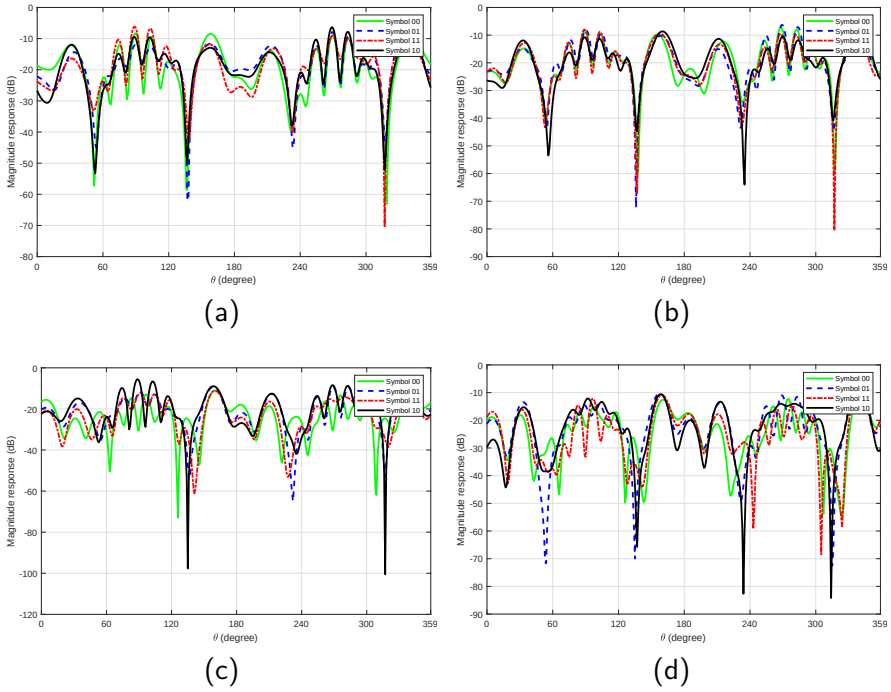

Figure 5: Resultant magnitude responses for eavesdroppers by the PM design in (15) at (a) $f_0 - 4 \triangle f$, (b) $f_0 - 2 \triangle f$, (c) f_0, (d) $f_0 + 2 \triangle f$.

obtained by the iterative optimisation method. Note that all phase values are optimized from the set $[0, \pi/2, \pi, 3\pi/2]$ and the set is obtained according to Eq. (13) when $B = 2$. Based on these values and the given parameters, the resultant magnitude patterns using Eq. (15) at frequencies $f_0 - 4 \triangle f$,

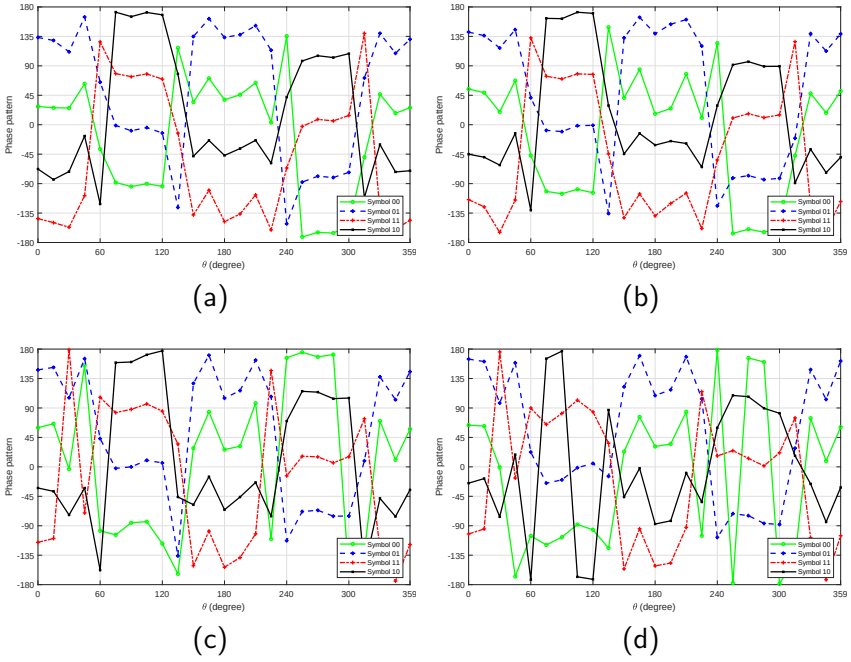

Figure 6: Resultant phase responses for eavesdroppers by the PM design in (15) at (a) $f_0 - 4 \triangle f$, (b) $f_0 - 2 \triangle f$, (c) f_0, (d) $f_0 + 2 \triangle f$.

$f_0 - 2 \triangle f$, f_0, $f_0 + 2 \triangle f$ are shown in Figs. 5a, 5b, 5c and 5d, and the corresponding phase patterns are displayed in Figs. 6a, 6b, 6c, 6d. Here, we can see that the magnitude response level at all eavesdroppers' locations is lower than that for the desired locations, and the phase of the received signal at these eavesdroppers is random. The magnitude and phase patterns at frequencies $f_0 - 3 \triangle f$, $f_0 - \triangle f$, $f_0 + \triangle f$, $f_0 + 3 \triangle f$ are not given as they have the same features as in the aforementioned figures. Fig. 7a shows the cost function value versus iteration number, and we can see that the cost function value is decreasing and does not change from the third iteration to the fifth iteration; in other words, the cost function has converged.

4.2. Design example for the single carrier based PM design

With the optimised phase value for each metasurface element, as shown in Fig 4b, the resultant magnitude and phase responses for the eavesdroppers are shown in Figs. 8 and 9, where the beam response level is lower than the desired receiver magnitude level 0dB, with random phase shifts at these eavesdroppers' locations. Fig. 7b shows the cost function value vs iteration

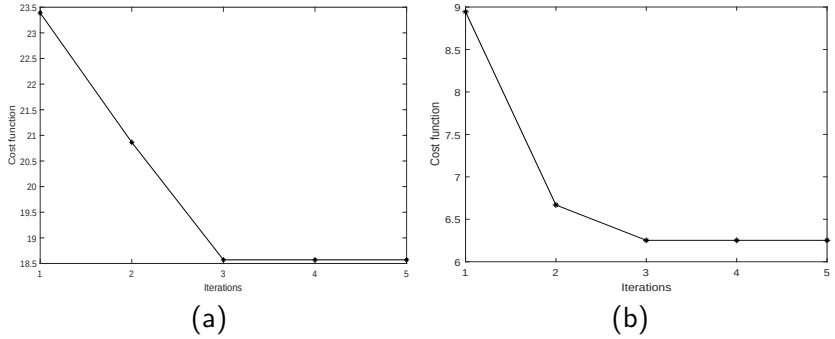

Figure 7: (a) Cost function vs Iterations in (15). (b) Cost function vs Iterations in (22).

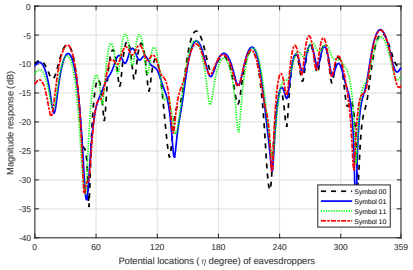

Figure 8: Resultant magnitude responses for eavesdroppers by the PM design in the single carrier case in (22).

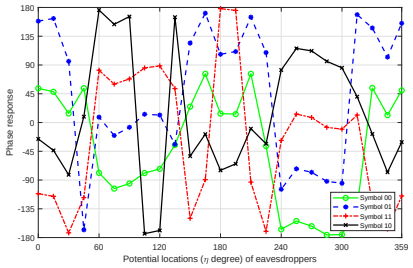

Figure 9: Resultant phase responses for eavesdroppers by the PM design in the single carrier case in (22).

number, and it can be seen that the cost function has converged after the third iteration.

5. Conclusions

In this paper, the multi-carrier based positional modulation design is proposed with discrete phase value constraint for metasurface elements, where multiple signals can be transmitted to the desired position(s) at multiple frequencies over a single channel simultaneously. More importantly, the discrete phase value constraint was considered for metasurface for its practical implementation. The single carrier based PM design was also provided as a special case of the multi-carrier based design. Two methods were introduced, where the iterative optimisation method has a much lower complexity of $(O(zBQ))$ than the exhaustive search method $(O(2^{BQ}))$. Magnitude and phase responses for the desired receiver and eavesdroppers' locations have been shown to demonstrate the effectiveness of the proposed design. This work can be extended to dynamic DM design, i.e., under the constraint of keeping the standard constellation map at the desired position, the constellation patterns of other positions are distorted and randomly updated, which will be a topic of our future work.

6. Acknowledgments

The work was supported by the Natural Science Foundation of China (62101383) and Tianjin Research Innovation Project for Postgraduate Students (2021YJSS208).

[1] A. Babakhani, D. B. Rutledge, and A. Hajimiri, "Near-field direct antenna modulation," *IEEE Microwave Magazine*, vol. 10, no. 1, pp. 36–46, February 2009.

[2] M. P. Daly and J. T. Bernhard, "Directional modulation technique for phased arrays," *IEEE Transactions on Antennas and Propagation*, vol. 57, no. 9, pp. 2633–2640, September 2009.

[3] B. Zhang, W. Liu, Q. Li, Y. Li, X. Zhao, C. Zhang, and C. Wang, "Directional modulation design under a given symbol-independent magnitude constraint for secure iot networks," *IEEE Internet of Things Journal*, vol. 8, no. 20, pp. 15 140–15 147, 2021.

[4] S. Feng, X. Ling, J. Wang, Z. Wei, and X. Zhou, "Artificial-noise-aided secure multicast precoding for directional modulation systems," *IEEE Transactions on Vehicular Technology*, vol. 67, no. 7, pp. 6658–6662, 2017.

[5] M. P. Daly and J. T. Bernhard, "Beamsteering in pattern reconfigurable arrays using directional modulation," *IEEE Transactions on Antennas and Propagation*, vol. 58, no. 7, pp. 2259–2265, March 2010.

[6] B. Zhang, W. Liu, Y. Li, X. Zhao, and C. Wang, "Directional modulation design under a constant magnitude constraint for weight coefficients," *IEEE Access*, vol. 7, pp. 154 711–154 718, 2019.

[7] ——, "Directional modulation design under maximum and minimum magnitude constraints for weight coefficients," *Ad Hoc Networks*, vol. 98, p. 102034, 2020. [Online]. Available: http://www.sciencedirect.com/science/article/pii/S1570870519307802

[8] R. M. Christopher and D. K. Borah, "Iterative convex optimization of multi-beam directional modulation with artificial noise," *IEEE Communications Letters*, vol. 22, no. 8, pp. 1712–1715, aug 2018.

[9] B. Zhang, W. Liu, and Q. Li, "Multi-carrier waveform design for directional modulation under peak to average power ratio constraint," *IEEE Access*, vol. 7, pp. 37 528–37 535, 2019.

[10] H. Z. Shi and A. Tennant, "Enhancing the security of communication via directly modulated antenna arrays," *IET Microwaves, Antennas & Propagation*, vol. 7, no. 8, pp. 606–611, June 2013.

[11] Y. Ding and V. Fusco, "Directional modulation transmitter radiation pattern considerations," *IET Microwaves, Antennas & Propagation*, vol. 7, no. 15, pp. 1201–1206, December 2013.

[12] Q. J. Zhu, S. W. Yang, R. L. Yao, and Z. P. Nie, "Directional modulation based on 4-D antenna arrays," *IEEE Transactions on Antennas and Propagation*, vol. 62, no. 2, pp. 621–628, February 2014.

[13] S. Wang, S. Yan, J. Zhang, N. Yang, R. Chen, and F. Shu, "Secrecy zone achieved by directional modulation with random frequency diverse array," *IEEE Transactions on Vehicular Technology*, vol. 70, no. 2, pp. 2001–2006, 2021.

[14] T. Shen, S. Zhang, R. Chen, J. Wang, J. Hu, F. Shu, and J. Wang, "Two practical random-subcarrier-selection methods for secure precise wireless transmissions," *IEEE Transactions on Vehicular Technology*, vol. 68, no. 9, pp. 9018–9028, 2019.

[15] W. Wang, H. C. So, and H. Shao, "Nonuniform frequency diverse array for range-angle imaging of targets," *IEEE Sensors Journal*, vol. 14, no. 8, pp. 2469–2476, 2014.

[16] Y. Ding, J. Zhang, and V. Fusco, "Frequency diverse array ofdm transmitter for secure wireless communication," *Electronics Letters*, vol. 51, no. 17, pp. 1374–1376, 2015.

[17] J. Hu, S. Yan, F. Shu, J. Wang, J. Li, and Y. Zhang, "Artificial-noise-aided secure transmission with directional modulation based on random frequency diverse arrays," *IEEE Access*, vol. 5, pp. 1658–1667, 2017.

[18] B. Zhang and W. Liu, "Positional modulation design based on multiple phased antenna arrays," *IEEE Access*, vol. 7, pp. 33 898–33 905, 2019.

[19] W. Zhang, M. Le, B. Li, J. Wang, and J. Peng, "Directional modulation-enhanced multiple antenna arrays for secure and precise wireless transmission," *Sensors*, vol. 19, no. 22, p. 4833, nov 2019.

[20] S. Tomita, Y. Miyake, I. Kashiwamura, K. Komatsu, N. H. Tran, H. Oguma, N. Izuka, S. Kameda, T. Takagi, and K. Tsubouchi, "Hybrid single-carrier and multi-carrier system: Improving uplink throughput with optimally switching modulation," in *21st Annual IEEE International Symposium on Personal, Indoor and Mobile Radio Communications*, 2010, pp. 2438–2443.

[21] H. Shi and A. Tennant, "Secure communications based on directly modulated antenna arrays combined with multi-path," in *2013 Loughborough Antennas & Propagation Conference (LAPC)*, 2013, pp. 582–586.

[22] C. L. Holloway, E. F. Kuester, J. A. Gordon, J. O'Hara, J. Booth, and D. R. Smith, "An overview of the theory and applications of metasurfaces: The two-dimensional equivalents of metamaterials," *IEEE Antennas and Propagation Magazine*, vol. 54, no. 2, pp. 10–35, April 2012.

[23] L. B. Wang, K. Y. See, J. W. Zhang, B. Salam, and A. C. W. Lu, "Ultrathin and flexible screen-printed metasurfaces for emi shielding applications," *IEEE Transactions on Electromagnetic Compatibility*, vol. 53, no. 3, pp. 700–705, Aug 2011.

[24] S. V. Hum and J. Perruisseau-Carrier, "Reconfigurable reflectarrays and array lenses for dynamic antenna beam control: A review," *IEEE Transactions on Antennas and Propagation*, vol. 62, no. 1, pp. 183–198, Jan 2014.

[25] C. Liaskos, S. Nie, A. Tsioliaridou, A. Pitsillides, S. Ioannidis, and I. Akyildiz, "A new wireless communication paradigm through software-controlled metasurfaces," *IEEE Communications Magazine*, vol. 56, no. 9, pp. 162–169, Sep. 2018.

[26] Y. Liu, L. Zhang, B. Yang, W. Guo, and M. A. Imran, "Programmable wireless channel for multi-user mimo transmission using meta-surface," in *2019 IEEE Global Communications Conference (GLOBECOM)*, 2019.

[27] L. Zhang, X. Q. Chen, S. Liu, Q. Zhang, J. Zhao, J. Y. Dai, G. D. Bai, X. Wan, Q. Cheng, G. Castaldi, V. Galdi, and T. J. Cui, "Space-Time-Coding Digital Metasurfaces," *Nature communications*, vol. 9, no. 1, p. 4334, Octorber 2018.

[28] Y. Chen, Y. Wang, J. Zhang, and Z. Li, "Resource allocation for intelligent reflecting surface aided vehicular communications," *IEEE Transactions on Vehicular Technology*, vol. 69, no. 10, pp. 12 321–12 326, 2020.

[29] B. Zhang, W. Liu, J. Ma, Z. Qi, J. Zhang, L. Han, Y. Li, X. Zhao, C. Zhang, and C. Wang, "Sparse antenna array based positional modulation design with a low-complexity metasurface," *IEEE Access*, vol. 8, pp. 177 640–177 646, 2020.

[30] B. Zhang and W. Liu, "Multi-carrier based phased antenna array design for directional modulation," *IET Microwaves, Antennas Propagation*, vol. 12, no. 5, pp. 765–772, April 2018.

[31] W. Yang, H. Li, M. Li, Y. Liu, and Q. Liu, "Channel estimation for practical irs-assisted ofdm systems," in *2021 IEEE Wireless Communications and Networking Conference Workshops (WCNCW)*, 2021.

[32] W. Cai, H. Li, M. Li, and Q. Liu, "Practical modeling and beamforming for intelligent reflecting surface aided wideband systems," *IEEE Communications Letters*, vol. 24, no. 7, pp. 1568–1571, 2020.

[33] M. C. Grant and S. P. Boyd, "Graph implementations for nonsmooth convex programs," in *Recent advances in learning and control*. Springer, 2008, pp. 95–110.

[34] C. Research, "CVX: Matlab software for disciplined convex programming, version 2.0 beta," http://cvxr.com/cvx, September 2012.